UDC 621.762
https://doi.org/10.17073/0021-3438-2024-1-55-69

Research article
Научная статья

Mechanical and tribological characteristics of nickel-rich $CoCrCu_xFeNi_2$ high entropy-alloys

A.D. Fedotov, S.K. Mukanov, B.Yu. Romanenko, P.A. Loginov, M.Ya. Bychkova, S.I. Rupasov

National University of Science and Technology "MISIS"
4 Bld. 1 Leninskiy Prosp., Moscow 119049, Russia

✉ Alexander D. Fedotov (sashok12221998@mail.ru)

Abstract: This research explores the potential to enhance the copper solubility limit in high-entropy alloys (HEAs) within the CoCrCuFeNi system by increasing the nickel content twofold and applying additional heat treatment. The $CoCrCu_xFeNi_2$ HEAs were synthesized through mechanical alloying of elemental powders followed by hot pressing. The study investigated the microstructure and phase composition of $CoCrCu_xFeNi_2$ HEAs in relation to varying copper concentrations (x = 0; 0.25; 0.5; 0.75; 1.0). The evaluation of the alloy matrix's chemical composition, which is based on the FCC solid solution, enabled the determination of copper solubility. It was found that doubling the nickel content, relative to the equiatomic ratio, facilitated the formation of HEAs with a homogenous FCC structure for copper concentrations up to $x \leq 0.75$. Further heat treatment of these HEAs resulted in an enhanced copper solubility of up to 17.5 at.%. The mechanical and tribological properties of $CoCrCu_xFeNi_y$ HEAs were also assessed, revealing significant improvements in tensile strength (ranging from 910 to 1045 MPa) and hardness (285–395 HV) for the $CoCrCu_xFeNi_2$ alloys. Despite the increased copper solubility limit, the heat treatment process caused a decline in mechanical properties by 35–50 %, attributed to grain size enlargement to 5.5 μm. The $CoCrCu_{0.75}FeNi_2$ and $CoCrCuFeNi_2$ alloys exhibited the lowest wear rates when tested against Al_2O_3 counterbody, with wear rates of $1{,}58 \cdot 10^{-5}$ and $1{,}48 \cdot 10^{-5}$ $mm^3/(N \cdot m)$, respectively.

Keywords: powder metallurgy, high-entropy alloys, mechanical properties, wear resistance, heat treatment, transmission electron microscopy, scanning electron microscopy.

Acknowledgments: The work was carried out with the financial support of the Russian Science Foundation (project No. 22-79-10144).
The authors express their gratitude to Dr. M.I. Petrzhik for assistance in studies of mechanical properties (hardness and elastic modulus).

For citation: Fedotov A.D., Mukanov S.K., Romanenko B.Yu., Loginov P.A., Bychkova M.Ya., Rupasov S.I. Mechanical and tribological characteristics of nickel-rich $CoCrCu_xFeNi_2$ high entropy-alloys. *Izvestiya. Non-Ferrous Metallurgy.* 2024;30(1):55–69.
https://doi.org/10.17073/0021-3438-2024-1-55-69

Механические и трибологические свойства высокоэнтропийных сплавов $CoCrCu_xFeNi_2$ с высоким содержанием никеля

А.Д. Федотов, С.К. Муканов, Б.Ю. Романенко, П.А. Логинов, М.Я. Бычкова, С.И. Рупасов

Национальный исследовательский технологический университет «МИСИС»
Россия, 119049, г. Москва, Ленинский пр-т, 4, стр. 1

✉ Александр Дмитриевич Федотов (sashok12221998@mail.ru)

Аннотация: Работа посвящена изучению возможности повышения предела растворимости меди в высокоэнтропийных сплавах (ВЭС) системы CoCrCuFeNi путем двукратного увеличения концентрации никеля и проведения дополнительной термической

обработки. ВЭС $CoCrCu_xFeNi_2$ изготовлены механическим легированием элементных порошковых смесей и их последующим горячим прессованием. Исследованы микроструктура и фазовый состав ВЭС $CoCrCu_xFeNi_2$ в зависимости от концентрации Cu (x = 0; 0,25; 0,5; 0,75; 1,0). Анализ химического состава матрицы сплава на основе ГЦК твердого раствора позволил определить растворимость меди. Показано, что двукратное (относительно эквиатомного) содержание никеля способствовало получению ВЭС с однофазной ГЦК-структурой при $x \leq 0{,}75$. Последующая термическая обработка ВЭС привела к увеличению растворимости меди до 17,5 ат.%. Проведены испытания механических и трибологических свойств ВЭС $CoCrCu_xFeNi_y$. В сплавах $CoCrCu_xFeNi_2$ достигнут высокий уровень прочности при растяжении (от 910 до 1045 МПа) и твердости (285–395 HV). Несмотря на повышение предела растворимости меди, термическая обработка привела к понижению механических свойств на 35–50 % из-за увеличения размера зерен до 5,5 мкм. Минимальным приведенным износом при трении в паре с контртелом из Al_2O_3 обладают сплавы $CoCrCu_{0,75}FeNi_2$ и $CoCrCuFeNi_2$ ($1{,}58 \cdot 10^{-5}$ и $1{,}48 \cdot 10^{-5}$ мм^3/(Н·м) соответственно).

Ключевые слова: порошковая металлургия, высокоэнтропийные сплавы, механические свойства, износостойкость, термическая обработка, просвечивающая электронная микроскопия, растровая электронная микроскопия.

Благодарности: Работа выполнена при финансовой поддержке Российского научного фонда (проект № 22-79-10144).

Авторы выражают благодарность д.т.н. М.И. Петржику за помощь в исследовании механических свойств (твердость и модуль упругости).

Для цитирования: Федотов А.Д., Муканов С.К., Романенко Б.Ю., Логинов П.А., Бычкова М.Я. , Рупасов С.И. Механические и трибологические свойства высокоэнтропийных сплавов $CoCrCu_xFeNi_2$ с высоким содержанием никеля. *Известия вузов. Цветная металлургия.* 2024;30(1):55–69. https://doi.org/10.17073/0021-3438-2024-1-55-69

Introduction

Over the past decade, high-entropy alloys (HEAs) based on the Co—Cr—Cu—Fe—Ni system have gained significant attention across various engineering disciplines [1—5] due to their exceptional mechanical properties at both ambient and elevated temperatures, coupled with remarkable thermal stability. These attributes render them ideal for critical applications such as combustion chambers and heat exchangers [6]. Their high corrosion resistance has led to their widespread adoption in the shipbuilding industry [7]. These alloys have been effectively utilized in coatings to enhance the corrosion resistance of magnesium alloy products [8]. Among their diverse uses, one of the most notable is in friction pair materials, attributed to their superior wear resistance at both room [9—11] and elevated temperatures [12; 13]. Collectively, the attributes of high wear resistance, ease of manufacturing, and low consolidation temperature when utilizing powder metallurgy methods render HEAs promising candidates as binders in diamond cutting tools [14; 15].

Extensive research has focused on the interplay between the mechanical properties and phase composition of CoCrCuFeNi high-entropy alloys (HEAs). These alloys can manifest as either a single-phase entity, comprising a substitutional solid solution with an FCC lattice structure, or a two-phase combination of FCC structures, contingent upon the concentration of copper [16]. Exceeding the solubility limit of copper results in a HEA structure characterized by a matrix FCC solid solution interspersed with copper-based interlayers also exhibiting an FCC structure [17—19]. Contemporary theories suggest that the inclusion of a copper phase diminishes the mechanical properties of CoCrCuFeNi HEAs and increases susceptibility to brittle fracture [20—24]. Alloys maintaining an equiatomic composition of cobalt, chromium, iron, and nickel can incorporate up to 9 at.% Cu while preserving a single-phase structure [18]. Therefore, broadening the copper concentration range that allows $CoCrCu_xFeNi$ HEAs to remain single-phase is a crucial objective, as achieving this would enable the development of HEAs with enhanced physical and mechanical characteristics, including improved strength, hardness, and wear resistance.

To augment the solubility of copper within the solid FCC solution, one strategy involves increasing the nickel content, which is uniquely characterized by its unlimited mutual solubility with copper within this family of HEAs, as evidenced by prior findings [25; 26]. Another approach is through heat treatment (HT), which stabilizes the structurally unstable state of HEAs typical at elevated temperatures, thereby enhancing the solubility of copper in the CoCrFeNi matrix.

This research aims to explore the potential of augmenting copper solubility in Co—Cr—Cu—Fe—Ni HEAs by increasing the nickel concentration and employing a supplementary quenching process. It entails a comparative analysis of the mechanical and tribological properties of equiatomic CoCrCuFeNi HEAs and the modified HEA with a doubled nickel content relative to the equiatomic ratio, designated as $CoCrCuFeNi_2$, which were obtained through quenching.

1. Materials and methods

The initial materials utilized in this study included carbonyl iron powder of grade VK-3 (Sintez-CIP LLC, Dzerzhinsk, Russia) with an average particle size of 9 μm and an impurity content of ≤0.3 wt.%, carbonyl nickel powder of grade PNK-UT3 (Kola MMC, Monchegorsk, Russia) with a particle size of 10 μm and impurity content of ≤0.06 wt.%, reduced cobalt powder of grade PK-1u (Hanrui Cobalt Co. LTD, China), with a particle size of 1.2 μm and impurity content of ≤0.03 wt.%, electrolytic chromium powder of grade PM-ERKh (AO Polema, Tula, Russia) with a particle size of 80 μm and impurity content of 0.05 wt.%, and electrolytic copper powder of grade PMS-1 (AO Uralelectromed, V. Pyshma, Russia) with a particle size of 24 μm and impurity content of 0.12 wt.%.

The base alloy for this study was $CoCrFeNi_2$, to which copper was added in varying mole fractions (0.25, 0.50, 0.75, and 1.0) relative to Co, Cr, and Fe. Powder mixtures were prepared using a planetary ball mill (PBM) "Activator-2sl" (Chemical Engineering Plant LTD, w.v. Dorogino, Novosibirsk region), under conditions optimized in prior research: a jar rotation speed of 694 rpm, a centrifugal factor of 90 *g*, for a duration of 30 min, and a ball to powder weight ratio of 15 : 1. To achieve finer particle sizes, the mixtures were further treated with 10 wt.% isopropyl alcohol in the same milling conditions for an additional 5 min, facilitating uniform distribution and mutual dissolution of Co, Cr, Cu, Fe, and Ni [17].

Cylindrical compact samples, 50 mm in diameter and 5 mm in height, were produced by hot pressing (HP) the $CoCrCu_xFeNi_2$ powder mixtures using a DSP-515 SA machine (Dr. Fritsch, Germany). The HP was conducted in a vacuum at a maximum temperature of 1100 °C, under a compaction pressure of 35 MPa, with an isobaric hold time of 3 min. After HP, the samples underwent additional HT in a protective hydrogen atmosphere at 1000 °C for 1.5 h.

Flat samples for tensile tests measuring 50 mm in total length with the working part dimensions of 20×5×2 mm, were fabricated from the compact samples using the electrical discharge cutting method.

The hardness of the hot-pressed samples was assessed using the Vickers method with an HVS-50 digital hardness tester (Time Group Inc., China) under a 10 kgf load. Hardness and elastic modulus measurements were also performed at the Testing Laboratory of Functional Surfaces (National scientific and educational center MISIS-ISMAN, Moscow, Russia) using a "Nano-Hardness Tester" (CSM Instruments, Switzerland). A Berkovich indenter (diamond triangular pyramid) was employed, applying an 8 mN load, with a loading speed of 0.36 mN/s, and a hold time at maximum load of 5 s.

Tensile tests were conducted on an "Instron 5966" universal testing machine (Instron, USA), with the ultimate tensile strength determined using the Bluehill software (Instron, USA).

The tribological behavior of the samples was evaluated using a "Tribometer" automated friction machine (CSM Instruments, Switzerland), employing a reciprocating motion based on the "Ball-on-Disc" configuration. The testing conditions included a track length of 6 mm, an applied load of 2 N, a maximum speed of 5 cm/s, and a sintered aluminum oxide (Al_2O_3) ball with a 3 mm diameter as the counterbody. The tests were run for 4000 cycles (covering 48 m) in air.

The microstructural analysis of both powdered and compacted materials was examined through scanning electron microscopy (SEM) using an S-3400N microscope (Hitachi, Japan), equipped with a "NORAN System 7 *X*-ray" energy-dispersive spectrometer (Thermo Scientific, USA). Further analysis of the materials' fine structure was conducted using a JEM 2100 transmission electron microscope (JEOL, Japan). Sample preparation for these analyses involved ion etching with a PIPS II system (Gatan, USA).

X-ray diffraction (XRD) analysis was performed using a "D2 Phaser" diffractometer (Bruker, USA) with CoK_α radiation, employing the Bragg—Brentano geometry over a 2θ range of 30 to 130°. Phase identification was facilitated by the Diffrac. EVA software (Bruker, USA). To refine the process for generating single-phase powders, XRD patterns of mixtures post 5, 10, 15, and 30 min of milling were analyzed, and the microstructure of their transversal cross-sections was examined.

2. Results and discussion

2.1. Fabrication of $CoCrCu_xFeNi_2$ alloy powders

To investigate phase formation processes during mechanical alloying (MA) of a Co—Cr—Cu—Fe—Ni powder mixture and to determine the optimal conditions for generating single-phase powders, XRD patterns of the mixtures after 5, 10, 15, and 30 min of treatment were examined, alongside analyses of their transversal cross-section microstructures.

Analysis after 5-minute treatment in the PBM revealed the presence of all phases corresponding to the starting powders (see Fig. 1 and Table 1), with the phase

weight content closely aligning with the theoretical calculations based on the mixture composition. As the treatment duration increased, a broadening of the diffraction peaks was observed, indicative of significant deformation within the crystallite lattices. Concurrently, a reduction in the peak intensities for Co, Cu, and Fe was noted.

The XRD pattern from the powder mixture after 15 min of PBM treatment, showed asymmetry in the Ni peaks from the (311) planes. This asymmetry suggests the formation of a new phase with an FCC lattice type, exhibiting lattice parameters slightly different from those of Ni (0.3570 and 0. 3525 nm, respectively).

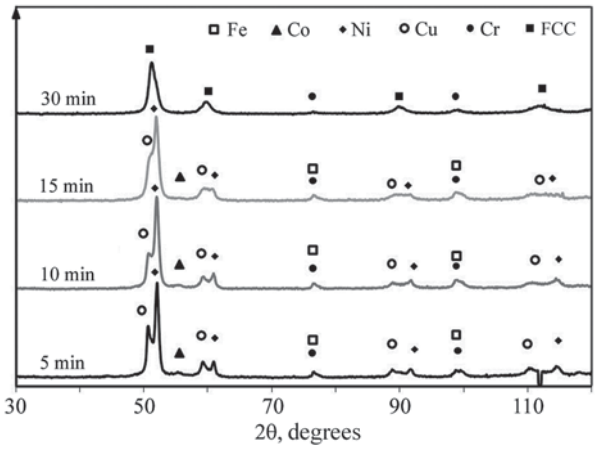

Fig. 1. XRD patterns of $CoCrCuFeNi_2$ alloy powders after PBM treatment

Рис. 1. Рентгенограммы порошковых смесей $CoCrCuFeNi_2$ после обработки в ПЦМ

Phase composition (wt.%) of Co–Cr–Cu–Fe–2Ni powder mixtures after mechanical alloying (MA) at various milling durations (τ_{MA})

Фазовый состав (мас.%) порошковых смесей Co–Cr–Cu–Fe–2Ni после механического легирования с различной продолжительностью ($\tau_{МЛ}$)

Phase (Pearson symbol)	τ_{MA}, min			
	5	10	15	30
Co (hP2/1)	12	8	6	–
Cr (cI2/1)	14	14	12	5
Cu (cF4/1)	16	12	10	–
Fe (cI2/1)	22	19	13	–
Ni (cF4/1)	36	47	47	–
FCC (cF4/1)	–	–	12	95

Following a 30-min treatment in the PBM, the powder predominantly consisted of an FCC solid solution with a minor presence of undissolved chromium (about 5 %). The residual chromium is not detrimental to the production of HEAs, as it is expected to dissolve into the matrix during the consolidation process through diffusion.

SEM studies on the structural evolution of the powder mixtures over different processing times revealed (Fig. 2) that due to the plastic nature of the components, structure formation during MA occurs via a mechanism typical for "ductile—ductile" systems. Under the impact of the grinding media, particles deform, creating new surfaces uncontaminated with oxygen, which form strong van der Waals bonds.

In the process of PBM, the initial metal particles tend to form large agglomerates (Fig. 2, *a*). These agglomerates exhibit a layered structure comprising distinguishable layers of Co, Cr, Cu, Fe, and Ni. The thickness of these metal layers varies with the particle size used in the process, typically ranging from 3—5 μm for Fe, Co, and Ni, to 20—30 μm for Cr and Cu (Fig. 2, *e*). As the milling process progresses, there is a notable gradual homogenization of the composite granules' structure (Fig. 2, *b*, *c*). expressed in a decrease in the thickness of the layers of metal components and their more chaotic arrangement. After τ_{MA} = 30 min, the resulting powders exhibit a homogeneous microstructure, with Cr present as submicron-thick interlayers (Fig. 2, *d*).

The fine structure of $CoCrCuFeNi_2$ alloy powders after 30-minute treatment in the PBM was examined using transmission electron microscopy (TEM). As shown in Fig. 3, the powders form complex-shaped agglomerates with a nanocrystalline structure exhibiting crystallite sizes ranging between 20—25 nm. Electron diffraction analysis of these particles identified diffraction rings consistent with the FCC phase. To further evaluate the alloy elemental homogeneity, EDS mapping was performed. The uniform intensity of characteristic *X*-ray emissions from Co, Cr, Cu, Fe, and Ni across the mapped area of the MA powder indicates a uniform distribution of these elements.

2.2. Analysis of CoCrCuxFeNi2 HEAs after HP and HP + HT

The consolidation of mechanically alloyed powder mixtures was achieved using the HP method, with some of the HP alloy samples undergoing additional treatments of annealing and hardening, referred to as HP + HT. The objective was to examine the copper solubility within the $CoCrCu_xFeNi_2$ HEA matrix, which

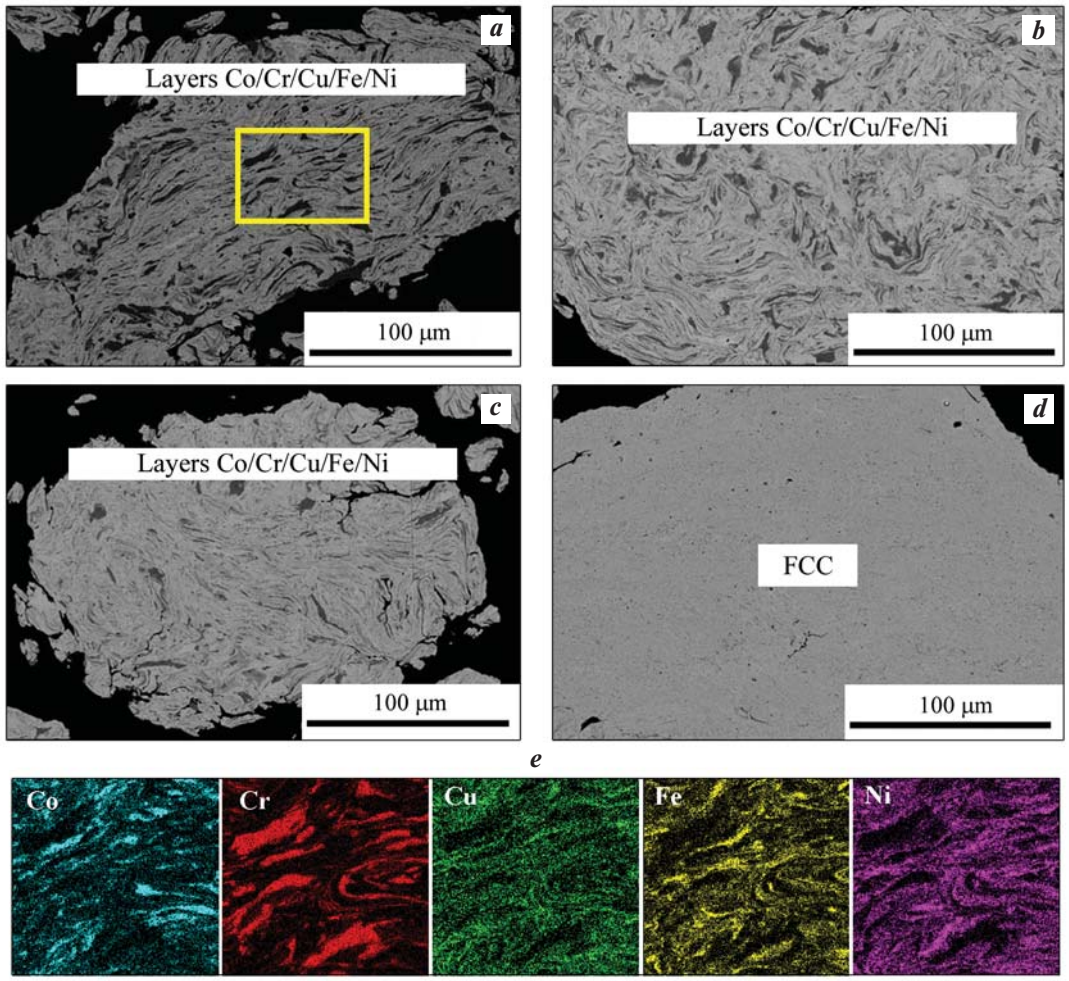

Fig. 2. Microstructures of $CoCrCuFeNi_2$ powder mixtures after PBM treatment at varied durations (***a–d***) and elemental distribution maps (***e***) derived from a particle treated for 5 min, corresponding to the region indicated in image ***a***
τ_{MA}, min: ***a*** – 5, ***b*** – 10, ***c*** – 15, ***d*** – 20

Рис. 2. Микроструктуры порошковых смесей $CoCrCuFeNi_2$ после обработки в ПЦМ с различной продолжительностью (***a–d***) и карты распределения элементов (***e***), снятые с частицы после 5 мин обработки, из выделенной на фото ***a*** области
$\tau_{МЛ}$, мин: ***a*** – 5, ***b*** – 10, ***c*** – 15, ***d*** – 20

involved analyzing the phase composition, microstructure, and the chemical composition of the different phases present.

XRD patterns presented in Fig. 4 showcase the structural outcomes for $CoCrCu_xFeNi_2$ HEAs after HP and HP + HT treatments. The primary structure identified in all HP-treated $CoCrCu_xFeNi_2$ HEA samples is an FCC solid solution that incorporates all alloy components, characterized by a cF4/1 structural type and a lattice parameter of 0.3577 nm. Previous studies indicated [17] that in $CoCrCu_xFeNi$ alloys, the formation of a secondary copper-based phase occurs at $x \geq 0.5$. In $CoCrCu_xFeNi_2$ alloys with an elevated nickel content, traces of this copper phase become apparent only at $x \geq 0.75$. The detection of this copper phase in $CoCrCu_{0,75}FeNi_2$ and $CoCrCuFeNi_2$ HP alloys was confirmed by low-intensity peaks on the lower angle (2θ) side of the XRD patterns (Fig. 4, inset).

Applying HT for HP samples of all $CoCrCu_xFeNi_2$ HEAs effectively prevents the emergence of the copper (Cu) phase across the board. Notably, even in the alloy with the highest copper content examined, $CoCrCuFeNi_2$, the anticipated peaks for the (Cu) phase were absent, illustrating that HT successfully maintains the $CoCrCuFeNi_2$ HEAs in a single-phase state at elevated temperatures (Fig. 4).

The microstructural characteristics of the compacted samples were explored using the SEM me-

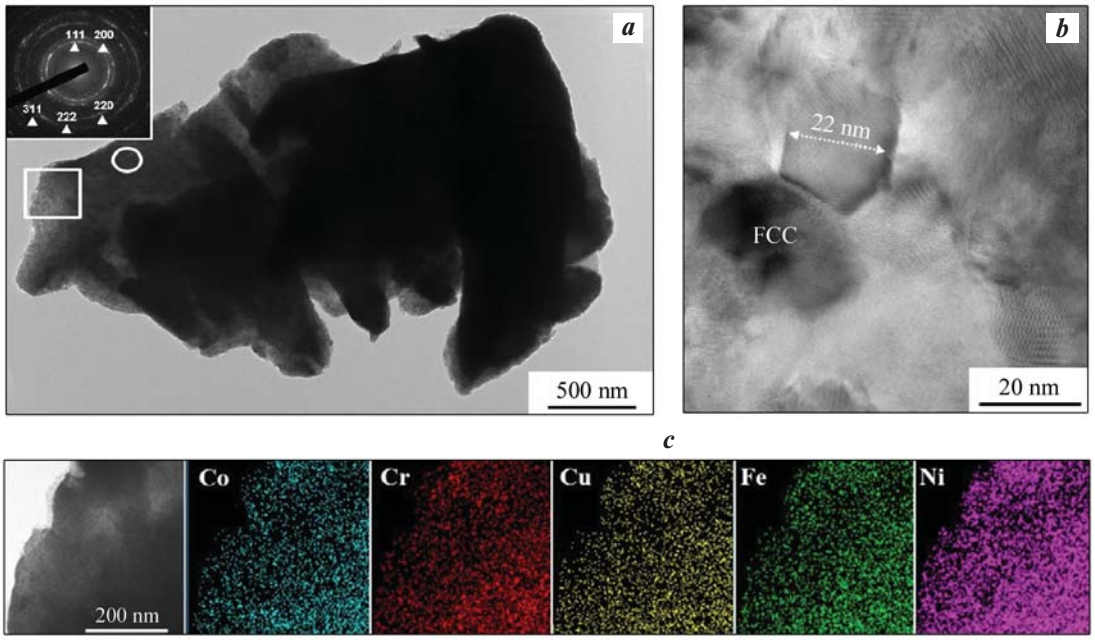

Fig. 3. Visualization of a $CoCrCuFeNi_2$ powder particle after 30 minutes PBM treatment (***a***); area within the white circle indicating the grain microstructure examination zone (***b***); white rectangle delineating the region analyzed via EDS (***c***)

Рис. 3. Изображение частицы порошка $CoCrCuFeNi_2$ после обработки в ПЦМ в течение 30 мин (***a***); область (белая окружность на рис. ***a***), в которой изучена зеренная микроструктура (***b***) и область (белый прямоугольник на рис. ***a***), в которой проводился ЭДС-анализ (***c***)

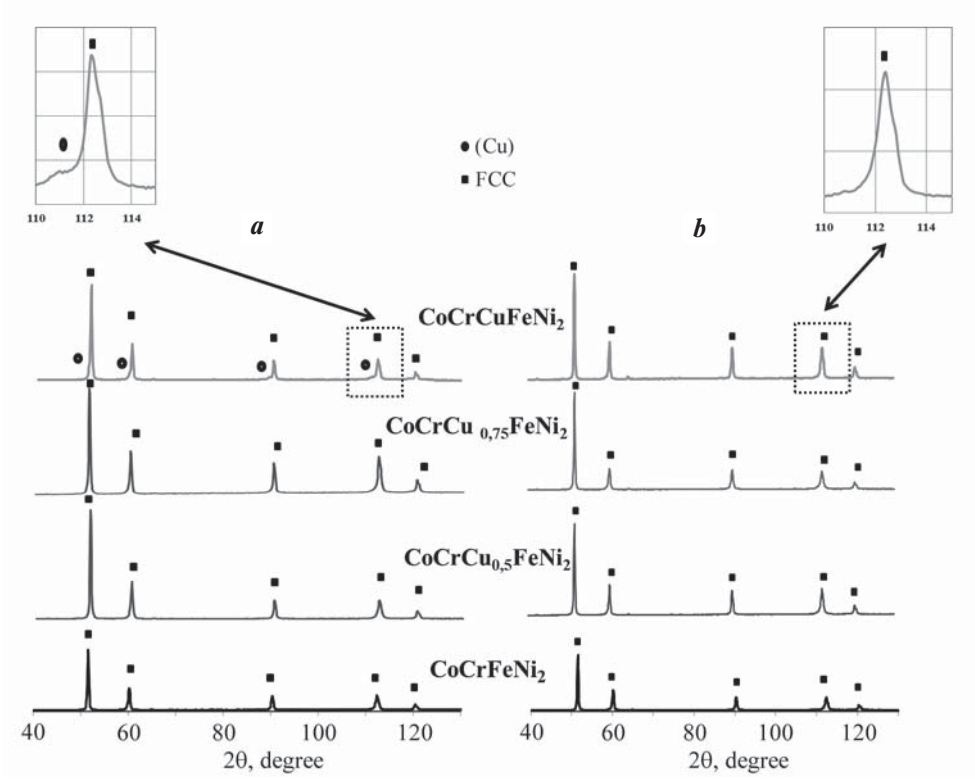

Fig. 4. XRD patterns of $CoCrCu_xFeNi_2$ HEAs after HP (***a***) and HP + HT (***b***)

Рис. 4. Рентгенограммы ВЭС $CoCrCu_xFeNi_2$ после ГП (***a***) и ГП + ТО (***b***)

thod (Fig. 5). It was determined that the matrix of all HP $CoCrCu_xFeNi_2$ HEA samples comprises a FCC solid solution phase. This phase uniformly incorporates submicron Cr_2O_3 oxide particles, which are not detectable by XRD due to their minimal concentration. The (Cu) phase grains only become visible at copper concentrations $x \geq 0.75$ (Fig. 5, *e*). In the $CoCrCuFeNi_2$ alloy, the (Cu) constitutes about 10 % of the material and manifests as polygonal grains located along the grain boundaries of the FCC matrix (Fig. 5, *g*).

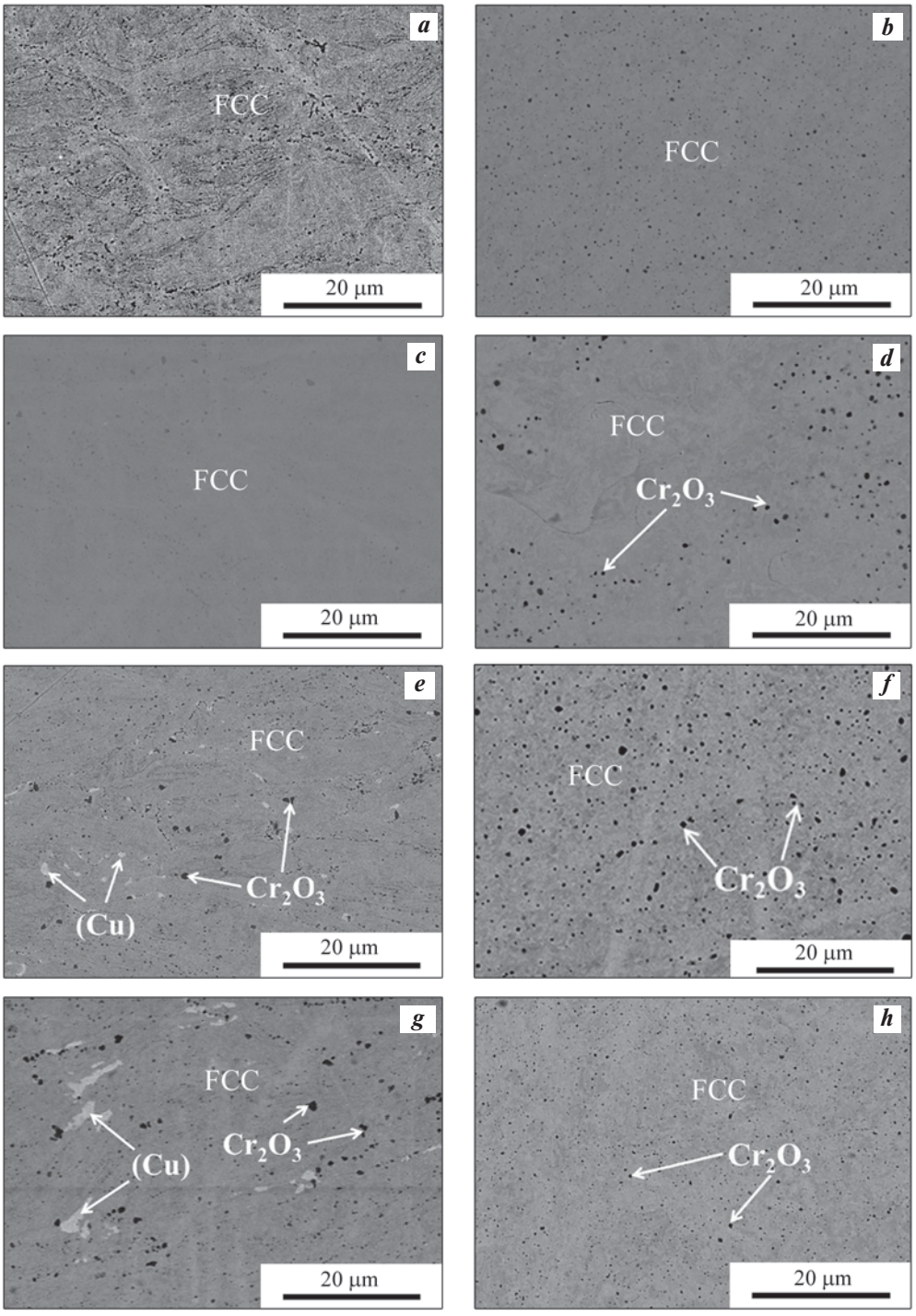

Рис. 5. Микроструктура ВЭС $CoCrCu_xFeNi_2$ после ГП (***a***, ***c***, ***e***, ***g***) и ГП + ТО (***b***, ***d***, ***f***, ***h***)
a, ***b*** – $CoCrFeNi_2$; ***c***, ***d*** – $CoCrCu_{0,5}FeNi_2$; ***e***, ***f*** – $CoCrCu_{0,75}FeNi_2$; ***g***, ***h*** – $CoCrCuFeNi_2$

Fig. 5. Microstructures of $CoCrCu_xFeNi_2$ HEAs after HP (***a***, ***c***, ***e***, ***g***) and HP + HT (***b***, ***d***, ***f***, ***h***)
a, ***b*** – $CoCrFeNi_2$; ***c***, ***d*** – $CoCrCu_{0.5}FeNi_2$; ***e***, ***f*** – $CoCrCu_{0.75}FeNi_2$; ***g***, ***h*** – $CoCrCuFeNi_2$

The HEAs subjected to HP + HT display a uniform microstructure, with the alloy matrix comprising solely of a FCC solid solution across all concentrations of Cu (Fig. 5, *b*, *d*, *f*, *h*).

TEM was employed to delve into the structural nuances of the $CoCrCuFeNi_2$ alloys afted HP and after HP + HT, with Fig. 6 presenting images at a uniform magnification to highlight the structural differences between these treatment stages. The HP-treated $CoCrCuFeNi_2$ alloy showcases an ultrafine-grained structure, evident from the bright-field image through the varied contrast across different regions, indicative of diverse crystallite orientations, and a ring-type diffraction pattern signaling a polycrystalline structure. The

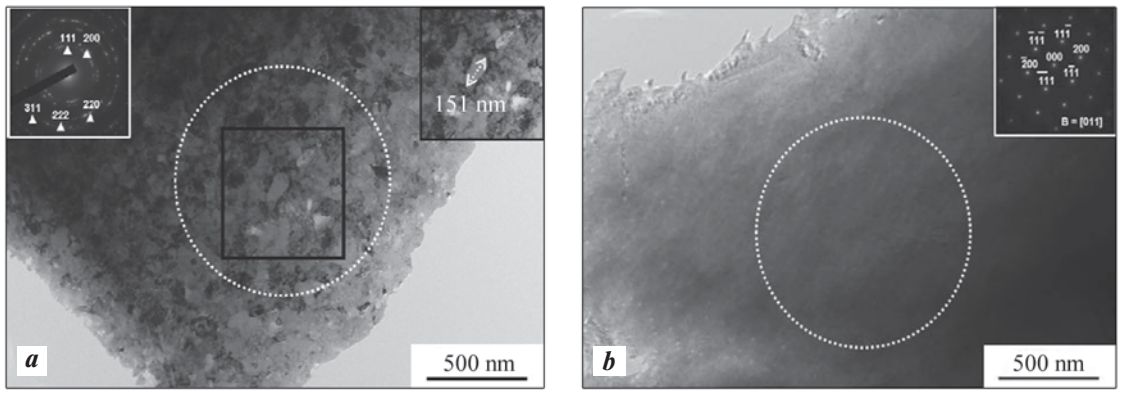

Fig. 6. Microstructure and electron diffraction pattern of $CoCrCuFeNi_2$ alloy samples after HP (***a***) and HP + HT (***b***)

Рис. 6. Микроструктура и электронная дифракция образцов сплава $CoCrCuFeNi_2$ после ГП (***a***) и ГП + ТО (***b***)

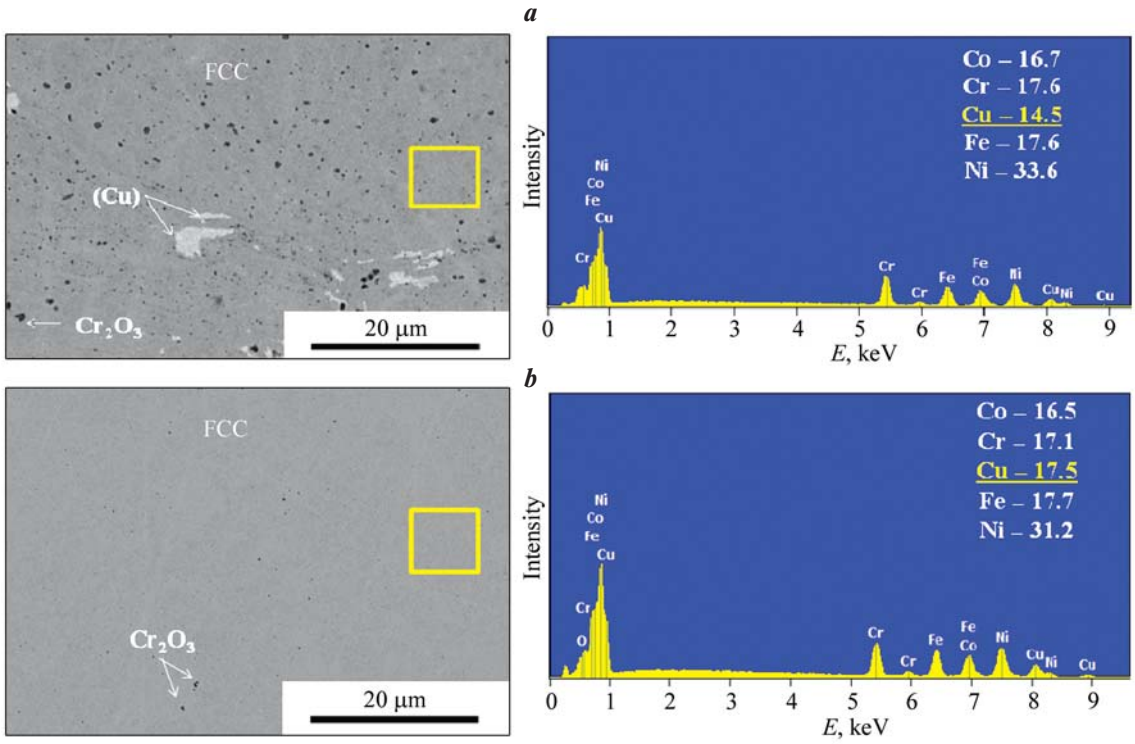

Fig. 7. Microstructures of $CoCrCuFeNi_2$ HEA after HP (***a***) and after HP + HT (***b***), including characteristic *X*-ray spectra from designated areas

Element concentrations presented in at.%

Рис. 7. Микроструктуры ВЭС $CoCrCuFeNi_2$ после ГП (***a***) и ГП + ТО (***b***) со спектрами характеристического рентгеновского излучения, снятыми с выделенных областей

Концентрации элементов указаны в ат.%

average grain size for the HP-treated $CoCrCuFeNi_2$ alloy is 150 nm (Fig. 6, *a*).

The application of HT to the $CoCrCuFeNi_2$ alloy induces a substantial increase in the grain size, a consequence of significant recrystallization activity. This is visualized in Fig. 6, *b* which displays a grain of the FCC phase nearly aligned with the [011] zone axis. Notably, within this grain, there are neither discernible grain boundaries nor inclusions of the (Cu) phase. This observation is in alignment with the findings from both XRD and SEM analyses. After undergoing the combined HP + HT process, the average grain size in the $CoCrCuFeNi_2$ alloy is recorded to be 5.5 μm.

The Co—Cr—Cu—Fe—Ni powder mixtures were subjected to high-energy mechanical treatment using PBM, resulting in a non-equilibrium phase composition, as outlined in Table 1. This process led to the formation of a supersaturated FCC solid solution, notably with copper among other components. Analysis of the chemical composition of the FCC phase after HP, which encouraged the formation of a thermodynamically stable structure through activated diffusion processes, allowed for the examination of copper solubility within the alloy matrix. The EDS analysis, conducted at 10 different points, yielded the average elemental concentrations in the FCC phase. Additionally, it provided visuals of a characteristic microstructure alongside EDS spectra, depicted in Fig. 7, *a*. The findings indicated that the solubility of copper in the FCC phase reached 14.5 at.%, which is 5.5 at.% higher than that in the equiatomic CoCrCuFeNi HEA [17].

Subsequent HT further augmented the solubility of copper in the matrix, achieving a concentration up to 17.5 at.% (Fig. 7, *b*).

2.3. Investigation of the mechanical characteristics of $CoCrCu_xFeNi_2$ HEAs

Figure 8 showcases the relationship between the hardness and tensile ultimate strength of $CoCrCu_xFeNi_2$ HEAs and the fraction of Cu present within them. The established trends from the test results reveal that the hardness of the HP samples increases linearly with the copper content, reaching a peak hardness of 395 HV for the $CoCrCuFeNi_2$ alloy. The hardness of HEAs after HP + HT is considerably less, ranging from 188 to 240 HV.

The indentation measurements (see Fig. 8, *c*) indicate that a rise in Cu content results in a reduction of hardness. This softening effect is likely due to the inclusion of the softer (Cu) phase. The process of heat treatment prompts grain growth, which in turn contributes to the deterioration of mechanical properties. However, it is important to note that the hardness variance in the HP + HT samples, relative to Cu concentration, falls within acceptable error margins, suggesting that the phase composition of these HEAs remains unchanged post-treatment.

In terms of tensile strength, the $CoCrCu_xFeNi_2$ HEAs produced via the HP method exhibit impressive values ranging from 910 to 1045 MPa (Fig. 8, *b*). These figures not only align with those of equiatomic $CoCrCu_xFeNi$ alloys obtained by powder metallurgy techniques [17] but also surpass the tensile strength of other similar alloys in the same system [27—30]. After HP + HT, the HEAs experience a 35—50 % reduction in tensile strength when compared to the HP-only alloys. This decline is attributed to the grain growth observed during the annealing phase of the heat treatment process (illustrated in Fig. 6) during the annealing process.

2.4. Study of wear resistance of $CoCrCu_xFeNi_2$ HEAs

Figure 9 illustrates the relationship between the friction coefficient and the number of cycles, including both 2D and 3D profiles of wear track. Data for comparison are also provided for alloys with a single-molar content of Ni as detailed in reference [17]. Despite variations in the Ni content and the application of HT, the friction coefficient remains relatively unchanged, falling within the range of 0.6 to 0.7. The fluctuations observed are likely due to the accumulation of wear debris between the surfaces in contact during tribological testing.

According to the data displayed in Fig. 10, a histogram delineates the reduced wear rate of $CoCrCu_xFeNi_2$ HEAs in relation to varying Cu concentrations.

For $CoCrCu_xFeNi_2$ HEAs obtained via the HP method, there is a discernible trend showing a decrease in reduced wear as the Cu content increases. This suggests a direct correlation between the hardness of the HEAs and their wear resistance. Specifically, the $CoCrCu_{0.75}FeNi_2$ and $CoCrCuFeNi_2$ alloys, which have the highest amounts of copper dissolved in the FCC matrix, exhibit the lowest wear rates under the conditions tested ($1.58 \cdot 10^{-5}$ and $1.48 \cdot 10^{-5}$ $mm^3/(N \cdot m)$, respectively).

The wear resistance of $CoCrCu_xFeNi_2$ HEAs processed through the HP+HT method is comparable or even superior to that of HP-only alloys at lower Cu concentrations. For Cu contents between 0.75 and 1.0 molar fractions, the wear resistance of the HP + HT alloys decreases by 2.5 to 3.0 times.

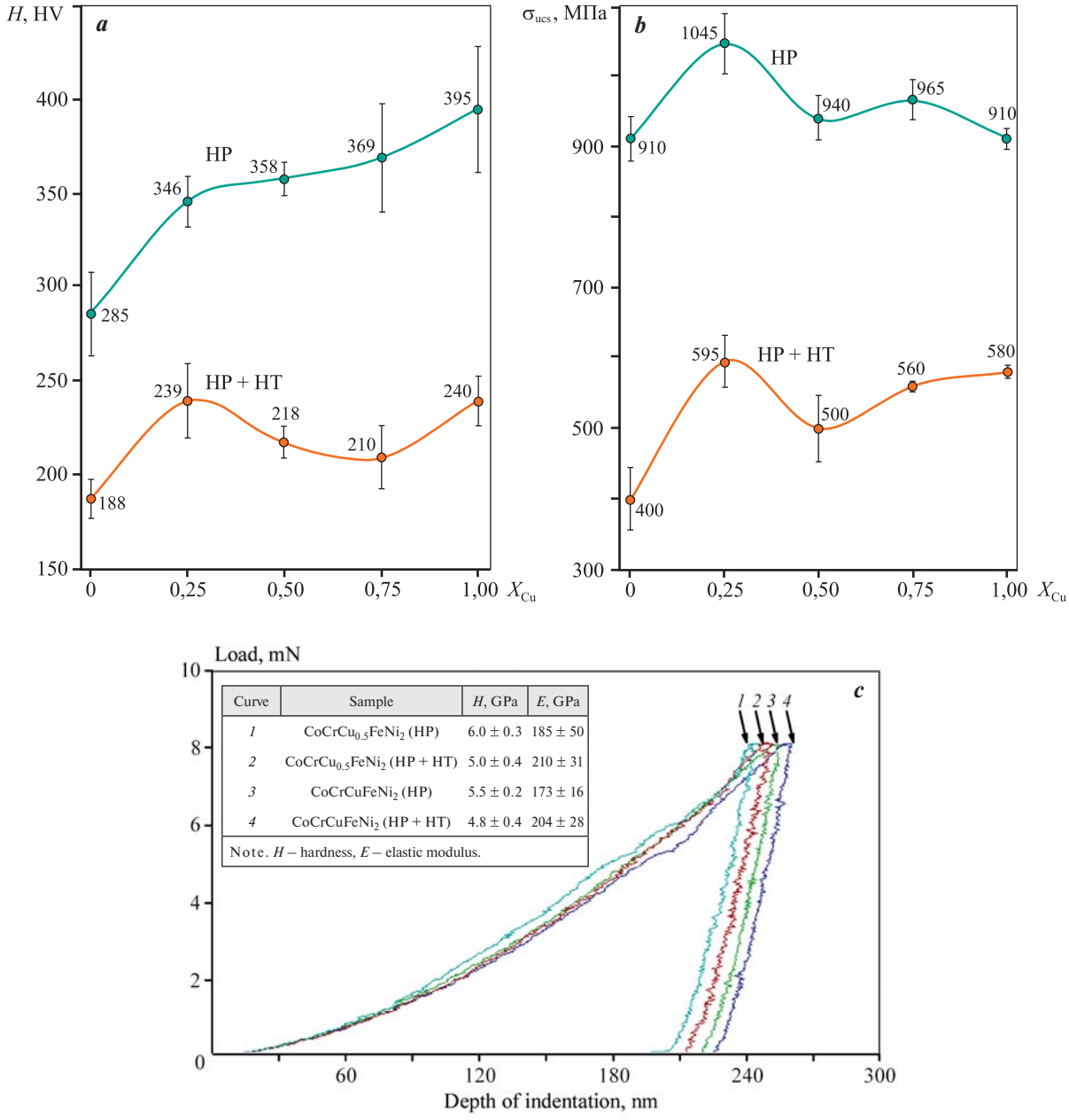

Fig. 8. Hardness (***a***), tensile strength (***b***) and measuring indentation (***c***) of $CoCrCu_xFeNi_2$ HEA

Рис. 8. Зависимости твердости (***a***) и предела прочности при растяжении (***b***) от концентрации меди в ВЭС $CoCrCu_xFeNi_2$ и результаты измерительного индентирования (***c***)

This lack of a clear trend can be attributed to the grain growth during the annealing phase of HT, which counteracts the beneficial effect of increased Cu concentration in the FCC matrix. This finding indicates that further research is necessary to optimize HT conditions for certain alloys.

The wear mechanism of HEAs was analyzed by examining wear tracks after testing (Fig. 11). Grooves marked by white arrows point in the direction of sliding of the Al_2O_3 counterbody, while dark gray regions identified by EDS consist of Ni and Fe oxides. These local oxidized areas are a result of frictional heating during the sliding process [31]. This oxidative wear mechanism, characterized by the presence of cracks perpendicular to the sliding direction, is common in HEAs with an FCC structure during dry friction with Al_2O_3 or Si_3N_4 balls [33]. The oxidation process initiates wear, leading to the detachment of oxidized fragments along the cracks (insets in Fig. 11, *a*), which con-

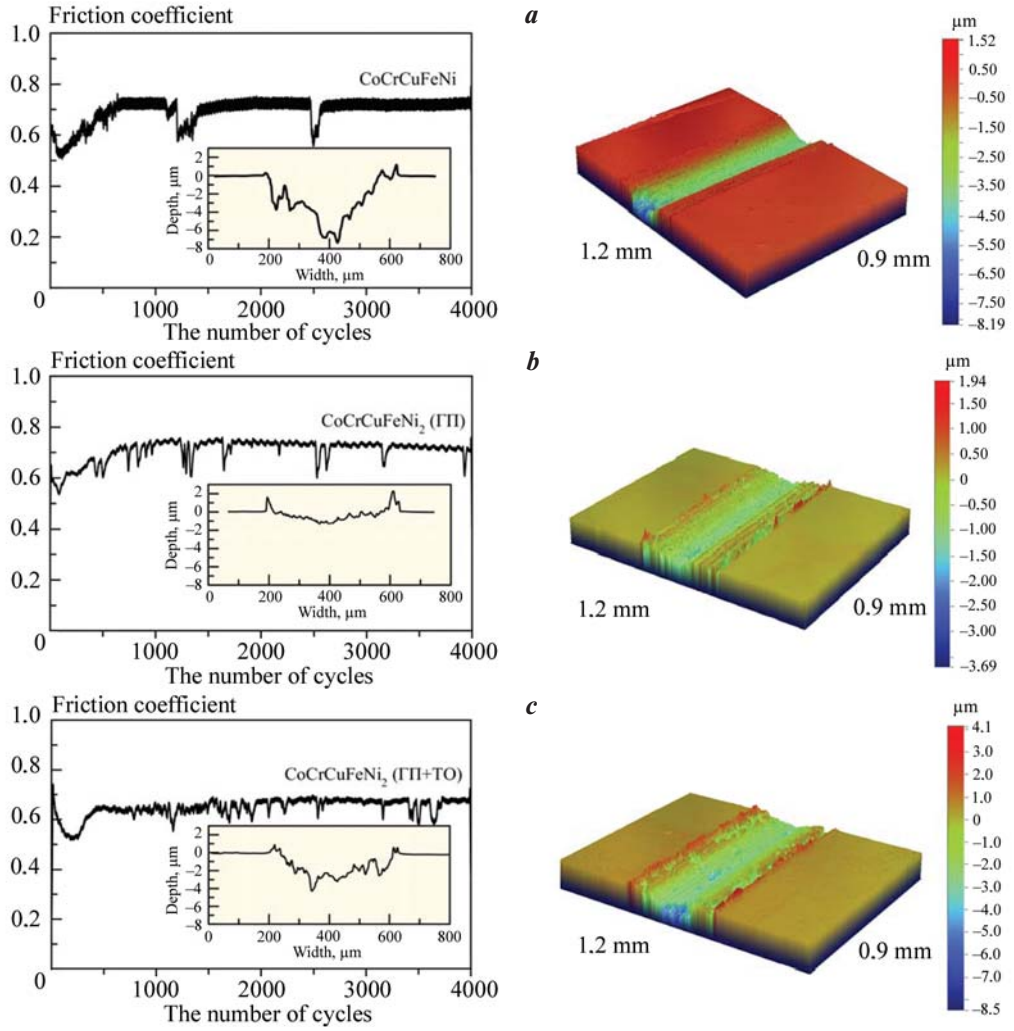

Fig. 9. Friction coefficient over cycle number with 3D and 2D representations of wear tracks in $CoCrCuFeNi_y$ HEAs
a – CoCrCuFeNi [17]; ***b*** – $CoCrCuFeNi_2$ (HP); ***c*** – $CoCrCuFeNi_2$ (HP + HT)

Рис. 9. Зависимость коэффициента трения от количества циклов и 3D- и 2D-изображения дорожек износа ВЭС $CoCrCuFeNi_y$
a – CoCrCuFeNi [17]; ***b*** – $CoCrCuFeNi_2$ (ГП); ***c*** – $CoCrCuFeNi_2$ (ГП + ТО)

tributes to the fluctuation of the friction coefficient (Fig. 9). Additionally, the solid wear debris causes micro-cutting of the sample, as evidenced by the grooves in the worn areas.

The study concludes that while the concentration of Cu in the HEAs and subsequent HT do not alter the wear mechanism, the hardness of the HEAs remains the key factor determining their wear resistance.

Conclusions

1. Compact samples of $CoCrCu_xFeNi_2$ HEAs were produced using MA and HP methods, resulting in either a single-phase FCC or a two-phase FCC + (Cu) structure.

2. It has been demonstrated that the solubility limit

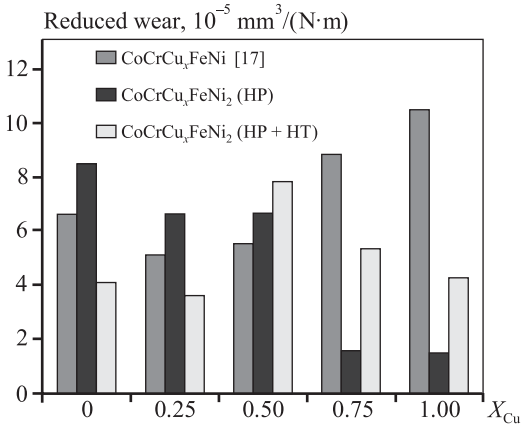

Fig. 10. Relationship between copper content and reduced wear rate in $CoCrCu_xFeNi_y$ HEAs

Рис. 10. Зависимость приведенного износа от содержания меди в ВЭС $CoCrCu_xFeNi_y$

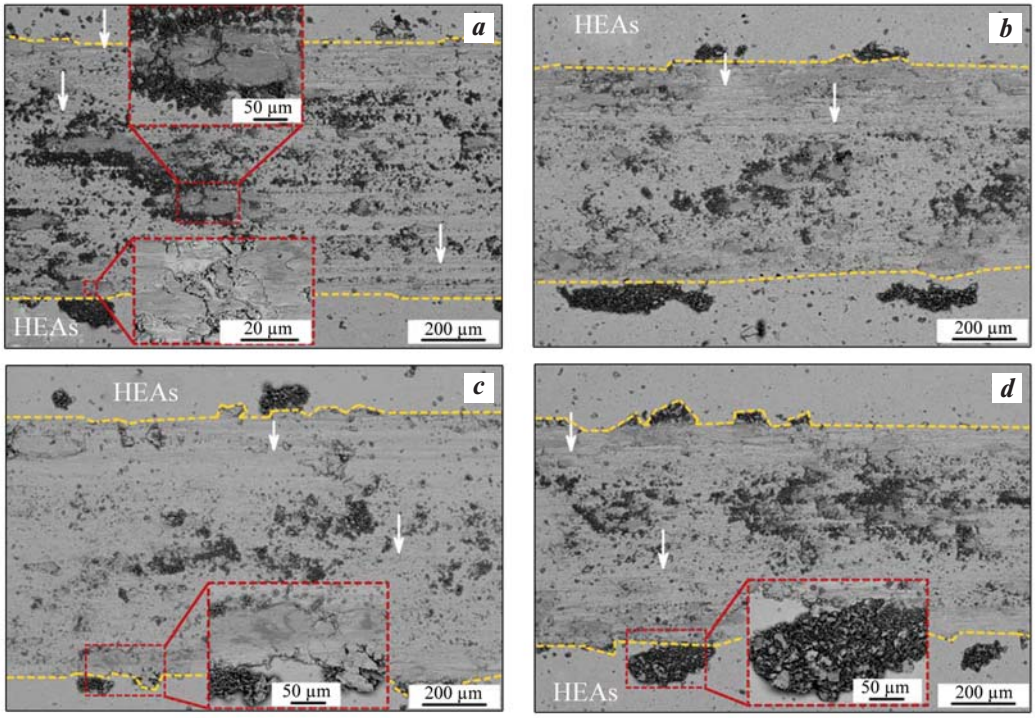

Fig. 11. SEM images of wear tracks on $CoCrCu_xFeNi_y$ HEAs
a – $CoCrCu_{0.5}FeNi_2$ (HP); ***б*** – $CoCrCu_{0.5}FeNi_2$ (HP + HT); ***в*** – $CoCrCuFeNi_2$ (HP); ***г*** – $CoCrCuFeNi_2$ (HP + HT)

Рис. 11. РЭМ-изображения дорожек износа ВЭС $CoCrCu_xFeNi_y$
а – $CoCrCu_{0,5}FeNi_2$ (ГП); ***б*** – $CoCrCu_{0,5}FeNi_2$ (ГП + ТО); ***в*** – $CoCrCuFeNi_2$ (ГП); ***г*** – $CoCrCuFeNi_2$ (ГП + ТО)

of Cu in the FCC solid solution can be increased from 9.0 at.% to 14.5 at.% by doubling the mole fraction of Ni in the $CoCrCu_xFeNi$ HEAs. This solubility is further enhanced to 17.5 at.% with the application of heat treatment, which includes annealing and quenching processes.

3. $CoCrCu_xFeNi_2$ HEAs obtained through the HP method exhibited high mechanical properties, with hardness values ranging between 285—395 HV and tensile strengths spanning 910 to 1045 MPa. However, heat treatment was found to reduce these mechanical properties, which is attributed to grain growth during isothermal annealing.

4. HEAs with a Cu content of 0.75—1.0 molar fractions, specifically those processed by HP, demonstrated high wear resistance ($1.48 \cdot 10^{-5}$ $mm^3/(N \cdot m)$) in friction tests with an Al2O3. The wear mechanism of the $CoCrCu_xFeNi_2$ HEAs involves oxidative processes combined with abrasive action.

References

1. Sanin V.N., Ikornikov D.M., Golosova O.A., Andreev D.E., Yukhvid V.I. Centrifugal metallothermic SHS of cast Co—Cr—Fe—Ni—Mn—(X) alloys. *Russian Journal of Non-Ferrous Metals*. 2020;61(4):436—445. https://doi.org/10.3103/S1067821220040070
2. Sanin V.N., Ikornikov D.M., Golosova O.A., Andreev D.E., Yukhvid V.I. Centrifugal SHS metallurgy of cast Co—Cr—Fe—Ni—Mn high-entropy alloys strengthened by precipitates based on Mo and Nb borides and silicides. *Physical Mesomechanics*. 2021;24: 692—700. https://doi.org/10.1134/S1029959921060072
3. Panina E.S., Yurchenko N.Y., Tozhibaev A.A., Mishunin M.V., Zherebtsov S.V., Stepanov N.D. A study of the structure and mechanical properties of Nb—Mo—Co—X (X = Hf, Zr, Ti) refractory high-entropy alloys. *Physical Mesomechanics*. 2023;26:666—677. https://doi.org/10.1134/S1029959923060061
4. Gromov V.E., Shlyarova Yu.A., Konovalov S.V., Vorob'ev S.V., Peregudov O.A. Application of high-entropy alloys. *Izvestiya. Ferrous Metallurgy.* 2021;64(10): 747—754. (In Russ.). https://doi.org/10.17073/0368-0797-2021-10-747-754
Громов В.Е., Шляпова Ю.А., Коновалов С.В., Воробьев С.В., Перегудов О.А. Применение высокоэнтропийных сплавов. *Известия высших учеб-*

ных заведений. Черная металлургия. 2021;64(10): 747—754.
https://doi.org/10.17073/0368-0797-2021-10-747-754

5. Jiaojiao Yia, Lin Yang, Mingqin Xu, Lu Wang. Investigation of a novel CoCrCuNiTi high entropy alloy on microstructure and mechanical properties. *Russian Journal of Non-Ferrous Metals*. 2021;62:197—205.
https://doi.org/10.3103/S1067821221020073
6. Rao K.R., Alshgari R.A., Bahajjaj A.A.A., Chakraborty S., Sinha S.K. Effects of nano scale Y_2O_3 additions on microstructural stability and mechanical properties of equiatomic CoCrCuFeNi based high entropy alloys. *Materials Chemistry and Physics*. 2023;296:127325.
https://doi.org/10.1016/j.matchemphys.2023.127325
7. Kuptsov K.A., Antonyuk M.N., Sheveyko A.N., Bondarev A.V., Ignatov S.G., Slukin P.V., Dwivedi P., Fraile A., Polcar T., Shtansky D.V.. High-entropy Fe—Cr—Ni—Co—(Cu) coatings produced by vacuum electro-spark deposition for marine and coastal applications. *Surface and Coatings Technology*. 2023;453:129136.
https://doi.org/10.1016/j.surfcoat.2022.129136
8. Huang K., Chen L., Lin X., Huang H., Tang S., Du F. Wear and corrosion resistance of $Al_{0.5}$CoCrCuFeNi high-entropy alloy coating deposited on AZ91D magnesium alloy by laser cladding. *Entropy*. 2018;20(12):915.
https://doi.org/10.3390/e20120915
9. Changqing Shu, Zhengjun Yao, Xiaolin Li, Wenbo Du, Xuewei Tao, Hemei Yang. Microstructure and wear mechanism of CoCrCuFeNiVx high entropy alloy by sintering and electron beam remelting. *Physica B: Condensed Matter*. 2022;638:413834.
https://doi.org/10.1016/j.physb.2022.413834
10. Kamalakannan R., DineshKumar K., NarenRaj K. The sliding wear behavior of CrCuFeNi alloyed with various combinations of cobalt. *Materials Today: Proceedings*. 2022;50(5):1814—1817.
https://doi.org/10.1016/j.matpr.2021.09.211
11. Verma A., Chauhan L., Kumar T.S., Singh Prashant Kumar, Dommeti Satya Gowtam, Thangaraju Shanmugasundaram. Laser cladding of CoCrCuFeNi and CoCrFeNi high-entropy alloys on DMR 249A steel: Corrosion, wear and antibacterial behaviour. *The Journal of the Minerals, Metals and Materials Society (TMS)*. 2023;75(7):2701—2713.
https://doi.org/10.1007/s11837-023-05861-z
12. Verma A., Tarate P., Abhyankar A.C., Mohape M.R., Gowtam D.S., Deshmukh V.P., Shanmugasundaram T. High temperature wear in CoCrFeNiCu_x high entropy alloys: The role of Cu. *Scripta Materialia*. 2019;171: 28—31.
https://doi.org/10.1016/j.scriptamat.2018.10.007
13. Yubin Huang, Yongle Hu, Mingjun Zhang, Cong Mao, Yonggang Tong, Jian Zhang, Kangwei Li, Kaiming Wang. On the enhanced wear resistance of laser-clad CoCrCuFeNiTi_x high-entropy alloy coatings at elevated temperature. *Tribology International*. 2022; 174:107767.
https://doi.org/10.1016/j.triboint.2022.107767
14. Yang Gao, Haibo Xiao, Bin Liu, Yong Liu. Enhanced drilling performance of impregnated diamond bits by introducing a novel HEA binder phase. *International Journal of Refractory Metals and Hard Materials*. 2024;118:106449.
https://doi.org/10.1016/j.ijrmhm.2023.106449
15. Loginov P.A., Fedotov A.D., Mukanov S.K., Manakova O.S., Zaitsev A.A., Akhmetov A.S., Rupasov S.I., Levashov E.A. Manufacturing of metal—diamond composites with high-strength CoCrCu_xFeNi high-entropy alloy used as a binder. *Materials*. 2023;16(3):1285
https://doi.org/10.3390/ma16031285
16. Takeshi Nagase, Philip D. Rack, Joo Hyon Noh, Takeshi Egami. In-situ TEM observation of structural changes in nano-crystalline CoCrCuFeNi multicomponent high-entropy alloy (HEA) under fast electron irradiation by high voltage electron microscopy (HVEM). *Intermetallics*. 2015;59:32—42.
https://doi.org/10.1016/j.intermet.2014.12.007
17. Mukanov S.K., Loginov P.A., Fedotov A.D., Bychkova M.Ya., Antonyuk M.N., Levashov E.A. The effect of copper on the microstructure, wear and corrosion resistance of CoCrCuFeNi high-entropy alloys manufactured by powder metallurgy. *Materials*. 2023;16(3):1178.
https://doi.org/10.3390/ma16031178
18. Shkodich N.F., Kovalev I.D., Kuskov K.V., Kovalev D.Yu., Vergunova Yu.S., Scheck Yu.B., Vadchenko S.G., Politano O., Baras F., Rogachev A.S. Fast mechanical synthesis, structure evolution, and thermal stability of nanostructured CoCrFeNiCu high entropy alloy. *Journal of Alloys and Compounds*. 2022;893:161839.
https://doi.org/10.1016/j.jallcom.2021.161839
19. Moghaddam A.O., Samodurova M.N., Pashkeev K., Doubenskaia M., Sova A., Trofimov E.A. A novel intermediate temperature self-lubricating CoCrCu_{1-x}FeNi_x high entropy alloy fabricated by direct laser cladding. *Tribology International*. 2021;156:106857.
https://doi.org/10.1016/j.triboint.2021.106857
20. Peng Jian, Li Zi-yong, Ji Xin-bo, Sun Yan-le, Fu Li-ming, Shan Ai-dang. Decomposition kinetics of carbon-doped FeCoCrNiMn high-entropy alloy at intermediate temperature. *Transactions of Nonferrous Metals Society of China*. 2020;30(7):1884—1894.
https://doi.org/10.1016/S1003-6326(20)65347-X
21. Dabrowa J., Cieslak G., Stygar M., Mroczka K., Berent K., Kulik T., Danielewski M. Influence of Cu content on high temperature oxidation behavior of AlCoCrCu$_x$FeNi

high entropy alloys (x = 0; 0.5; 1). *Intermetallics*. 2017; 84:52—61. https://doi.org/10.1016/j.intermet.2016.12.015
22. Li Cheng, Xue Yun-fei, Hua Mu-tian, Cao Tang-qing, Ma Li-li, Wang Lu. Microstructure and mechanical properties of $Al_xSi_{0.2}CrFeCoNiCu_{1-x}$ high-entropy alloys. *Materials and Design*. 2016;90:601—609. https://doi.org/10.1016/j.matdes.2015.11.013
23. Lin C.M., Tsai H.L. Equilibrium phase of high-entropy $FeCoNiCrCu_{0.5}$ alloy at elevated temperature. *Journal of Alloys and Compounds*. 2010;489(1):30—35. https://doi.org/10.1016/j.jallcom.2009.09.041
24. Lin C.M., Tsai H.-L. Effect of annealing treatment on microstructure and properties of high-entropy $FeCoNiCrCu_{0.5}$ alloy. *Materials Chemistry and Physics*. 2011;128(1-2):50—56. https://doi.org/10.1016/j.matchemphys.2011.02.022
25. Fangyan Liu, Qiang Song, Ruirun Chen, Canming Wang, Jiawei Sun. Effect of Co, Ni, Cu content on phase composition, microstructure and corrosion resistance of $Co_{1-x}CrFeNi_{1+x}Cu_y$ series high-entropy alloys. *Vacuum*. 2013;210:111830. https://doi.org/10.1016/j.vacuum.2023.111830
26. Zhu Z.G., Ma K.H., Wang Q., Shek C.H. Compositional dependence of phase formation and mechanical properties in three CoCrFeNi—(Mn/Al/Cu) high entropy alloys. *Intermetallics*. 2016;79:1—11. https://doi.org/10.1016/j.intermet.2016.09.003
27. Qiang Hu, Hai-ling Wang, Li-hua Qian, Liang-cai Zeng, Qiang Wang, Xin-wang Liu. Effects of Cu additions on microstructure and mechanical properties of as-cast $CrFeCoNiCu_x$ high-entropy alloy. *Transactions of Nonferrous Metals Society of China*. 2023;33(6):1803—1813. https://doi.org/10.1016/S1003-6326(23)66223-5
28. Du C., Hu L., Pan Q., Chen K., Zhou P., Wang G. Effect of Cu on the strengthening and embrittling of an FeCoNiCr—xCu HEA. *Materials Science and Engineering: A*. 2023;832:142413. https://doi.org/10.1016/j.msea.2021.142413
29. Fiocchi Jacopo, Casati Riccardo, Tuissi Ausonio, Biffi Carlo Alberto. Laser beam welding of CoCuFeMnNi high entropy alloy: Processing, microstructure, and mechanical properties. *Advanced Engineering Materials*. 2022;24(10):202200523. https://doi.org/10.1002/adem.202200523
30. Seung Min Oh, Sun Ig Hong. Microstructural stability and mechanical properties of equiatomic CoCrCuFeNi, CrCuFeMnNi, CoCrCuFeMn alloys. *Materials Chemistry and Physics*. 2018;210:120—125. https://doi.org/10.1016/j.matchemphys.2017.09.010
31. Fei Liang, Ao Meng, Yixing Sun, Zhaoshuo Chen, Zhouwen Jiang, Yaping Zhang, Yong Zhang, Yuntian Zhu, Xiang Chen. A novel wear-resistant Ni-based superalloy via high Cr-induced subsurface nanotwins and heterogeneous composite glaze layer at elevated temperatures. *Tribology International*. 2023;183:108383. https://doi.org/10.1016/j.triboint.2023.108383
32. Zhuo Cheng, Lu Yang, Zhikun Huang, Tian Wan, Mingyu Zhu, Fuzeng Ren. Achieving low wear in a μ-phase reinforced high-entropy alloy and associated subsurface microstructure evolution. *Wear*. 2021;474-475:203755. https://doi.org/10.1016/j.wear.2021.203755
33. Qiang Wang, Qiang Hu, Hailing Wang, Liangcai Zeng. Investigations on the microstructures and tribological behaviors of as-cast $CrFeCoNiCu_x$ high entropy alloys. *Intermetallics*. 2023;157:107886. https://doi.org/10.1016/j.intermet.2023.107886

Information about the authors

Alexander D. Fedotov – Postgraduate Student, Scientific Project Engineer, Department of Powder Metallurgy and Functional Coatings (PM&FC), National University of Science and Technology "MISIS" (NUST MISIS).
https://orcid.org/0009-0009-9208-1453
E-mail: sashok12221998@mail.ru

Samat K. Mukanov – Cand. Sci. (Eng.), Research Assistant, Laboratory "In situ diagnostics of structural transformations" of Scientific-Educational Center of SHS of MISIS–ISMAN.
https://orcid.org/0000-0001-6719-6237
E-mail: sam-mukanov@mail.ru

Информация об авторах

Александр Дмитриевич Федотов – аспирант, инженер научного проекта, кафедра порошковой металлургии и функциональных покрытий (ПМиФП), Национальный исследовательский технологический университет «МИСИС» (НИТУ МИСИС).
https://orcid.org/0009-0009-9208-1453
E-mail: sashok12221998@mail.ru

Самат Куандыкович Муканов – к.т.н., мл. науч. сотрудник, лаборатория «In situ диагностика структурных превращений» Научно-учебного центра (НУЦ) СВС МИСИС–ИСМАН.
https://orcid.org/0000-0001-6719-6237
E-mail: sam-mukanov@mail.ru

Bogdan Yu. Romanenko – Graduate Student, Training Master, Department of PM&FC, NUST MISIS.
https://orcid.org/0009-0003-7470-5185
E-mail: a.v.d.romanenko@gmail.com

Pavel A. Loginov – Cand. Sci. (Eng.), Assistant Prof. of NUST MISIS; Senior Researcher at the Laboratory "In situ diagnostics of structural transformations" of Scientific-Educational Center of SHS of MISIS–ISMAN.
https://orcid.org/0000-0003-2505-2918
E-mail: loginov.pa@misis.ru

Marina Ya. Bychkova – Cand. Sci. (Eng.), Assistant Prof. of NUST MISIS; Researcher Researcher at the Laboratory "In situ diagnostics of structural transformations" of Scientific-Educational Center of SHS of MISIS–ISMAN.
https://orcid.org/0000-0002-9233-4707
E-mail: bychkova@shs.misis.ru

Sergey I. Rupasov – Leading Expert of the scientific project, Department of PM&FC, NUST MISIS.
https://orcid.org/0000-0003-0948-688X
E-mail: rupasov@misis.ru

Богдан Юрьевич Романенко – магистр, учебный мастер, кафедра ПМиФП, НИТУ МИСИС.
https://orcid.org/0009-0003-7470-5185
E-mail: a.v.d.romanenko@gmail.com

Павел Александрович Логинов – к.т.н., доцент НИТУ МИСИС, ст. науч. сотрудник лаборатории «In situ диагностика структурных превращений» НУЦ СВС МИСИС–ИСМАН.
https://orcid.org/0000-0003-2505-2918
E-mail: loginov.pa@misis.ru

Марина Яковлевна Бычкова – к.т.н., доцент НИТУ МИСИС, науч. сотрудник НУЦ СВС МИСИС–ИСМАН.
https://orcid.org/0000-0002-9233-4707
E-mail: bychkova@shs.misis.ru

Сергей Иванович Рупасов – вед. эксперт научного проекта, кафедра ПМиФП, НИТУ МИСИС.
https://orcid.org/0000-0003-0948-688X
E-mail: rupasov@misis.ru

Contribution of the authors

A.D. Fedotov – planned the experiment, processed the experimental data, wrote the manuscript.

S.K. Mukanov – carried out tribological tests, participated in the discussion of the results.

B.Yu. Romanenko – prepared powder mixtures, processed the obtained results.

P.A. Loginov – formulated the general concept of the study, set the research goals, performed transmission electron microscopy experiments, and engaged in result discussions.

M.Ya. Bychkova – analyzed the experimental data and contributed to manuscript preparation.

S.I. Rupasov – executed sample compaction and performed mechanical testing (tension, bending).

Вклад авторов

А.Д. Федотов – планирование экспериментов, обработка экспериментальных данных, написание статьи.

С.К. Муканов – проведение трибологических испытаний, участие в обсуждении результатов.

Б.Ю. Романенко – приготовление порошковых смесей, обработка полученных результатов.

П.А. Логинов – разработка общей концепции статьи, определение цели работы, проведение экспериментов по просвечивающей электронной микроскопии, участие в обсуждении результатов.

М.Я. Бычкова – анализ экспериментальных данных, подготовка текста.

С.И. Рупасов – компактирование образцов, проведение механических испытаний (растяжение, изгиб).

The article was submitted 29.01.2024, accepted for publication 02.02.2024
Статья поступила в редакцию 29.01.2024, подписана в печать 02.02.2024